Energetics of Intermediates and Reaction Steps Involved in the Hydroformylation Reaction Catalyzed by $HCo(CO)_4$. A Theoretical Study Based on Density Functional Theory

Louis Versluis,[†] Tom Ziegler,*[,†] E. J. Baerends,[‡] and W. Ravenek[‡]

Contribution from the Department of Chemistry, University of Calgary, Calgary, Alberta, Canada T2N 1N4, and Department of Theoretical Chemistry, The Free University of Amsterdam, Amsterdam, The Netherlands. *Received July 6, 1988*

Abstract: A theoretical study based on density functional theory has been carried out on the CO dissociation of $HCo(CO)_4$ and the migratory insertion reaction $RCo(CO)_4 \rightarrow RC(O)Co(CO)_3$ for R = H and R = CH_3, respectively. $RCo(CO)_4$ was shown to form two stable isomers of trigonal-bipyramidal geometry. The configuration with R in axial position was lower in energy (63 kJ mol^{-1} for R = H and 42 kJ mol^{-1} for R = CH_3) than the corresponding isomer with R along the basal axis. The Co–CO dissociation energy of $HCo(CO)_4$ was found to be 186 kJ mol^{-1}. The resulting intermediate $HCo(CO)_3$ had as its most stable conformation a butterfly structure with the hydride in apical position. The migratory insertion of CO into the Co–CH_3 bond affords a coordinatively unsaturated acyl intermediate $CH_3C(O)Co(CO)_3$ that was found to form several stable isomers, with the ones that have the acyl oxygen facing the vacant site lowest in energy due to the formation of stable η^2 interactions. The reaction profile of the migration process was investigated by a linear transit procedure. The methyl 1,2-shift reaction to a *cis*-carbonyl group was found to have a low activation barrier and a reaction enthalpy of not more than 70 kJ mol^{-1}, whereas the direct insertion of a CO ligand into the Co–CH_3 bond was disfavored by an activation barrier of ~200 kJ mol^{-1}. The corresponding hydride migration to a neighboring CO group was considerably more endothermic and did not produce stable formyl intermediates on the Hartree–Fock–Slater energy surface. The alternative isomers with the formyl oxygen pointing toward the empty site were found to be stable but high in energy. Finally, an examination of the coordinatively saturated complex $RC(O)Co(CO)_4$ (R = H, CH_3) revealed that the neutral formyl compound is thermodynamically unstable with respect to decarbonylation to $HCo(CO)_4$. The reaction was found to have an exothermicity of ΔH = −69 kJ mol^{-1}, whereas the acyl complex was found to be stable with ΔH = 20 kJ mol^{-1} for the corresponding decarbonylation process of $CH_3C(O)Co(CO)_4$ to $CH_3Co(CO)_4$.

I. Introduction

The oxo or hydroformylation reaction is one of the few processes in which homogeneous catalysts are employed[1] on an industrial scale. Olefins and synthesis gas are in the hydroformylation reaction converted into aldehydes with cobalt and rhodium complexes as catalysts. The most commonly used (pre)catalyst is $HCo(CO)_4$, which is generated in situ from the hydrogenation of $Co_2(CO)_8$ by H_2. However, (pre)catalysts derived from $HCo(CO)_4$ by replacing one or more CO groups with phosphines, or cobalt with rhodium, have also been employed.[2]

Heck and Breslow[3] have proposed a reaction mechanism for the hydroformylation reaction in which $HCo(CO)_4$ is employed (see Figure 1). The first key step (a of Figure 1) in the mechanism of Heck and Breslow is the formation of the catalytic active species $HCo(CO)_3$ by the dissociation of a CO ligand from $HCo(CO)_4$. The unsaturated 16-electron tricarbonyl forms in the second step of the catalytic cycle a π-complex with olefin (b of Figure 1), from which the alkyl complex $RCo(CO)_4$ (R = alkyl) is generated by a migratory insertion process followed by the addition of a CO ligand (c of Figure 1). The next step (d of Figure 1) in the catalytic cycle involves the intramolecular migration of the alkyl group R to a *cis*-carbonyl ligand, affording the coordinatively unsaturated acyl complex $R(O)C–HCo(CO)_3$. The cycle is finally completed in step e of Figure 1 where the acyl complex reacts with H_2 to produce the aldehyde as well as the regenerated catalyst $HCo(CO)_3$.

Migratory insertions and CO dissociations are common and well-studied[4,5] reaction steps in organometallic chemistry. Nevertheless, experimental studies of the actual elementary reactions in the catalytic cycle of Figure 1 have proven to be difficult. The energetics of each of the steps a–e is as a consequence not well established nor are the structures of the involved species, with the exception of $HCo(CO)_4$,[6] known in any detail.

There have over the years been several theoretical studies[4d,7] relating to the hydroformylation process, partly as a result of its importance and partly due to the relatively modest size of the involved species. Most of the theoretical investigations have concentrated on the electronic structure[7b–f,8] of one or more of the species in Figure 1. Structural optimizations on some of the systems in the catalytic cycle have also been performed.[4d,7a,8] However, the optimizations have, with the exception of the recent work by Antolovic and Davidson,[8] been restrained to a few key parameters. The ab initio Hartree–Fock (HF) study by Antolovic and Davidson (AD) represents to date the most comprehensive theoretical investigation of the steps a–d in the hydroformylation process. However, AD modeled the crucial migratory insertion step d by replacing the alkyl group R with hydride. This might not be entirely appropriate since hydride is known to have a much poorer migratory aptitude toward CO than alkyl.[4e] Furthermore, the ab initio HF method is known not to provide reliable M–CO bond distances and bond dissociation energies, as discussed by AD[8] and others.[9]

[†] University of Calgary.
[‡] The Free University of Amsterdam.

(1) (a) Heck, R. F. *Adv. Organomet. Chem.* **1966**, *4*, 243. (b) Orchin, M.; Rupilius, W. *Catal. Rev.* **1972**, *6*, 85. (c) Orchin, M. *Acc. Chem. Res.* **1981**, *14*, 259.
(2) Pino, P.; Piacenti, F.; Bianchi, M. In *Organic Synthesis via Metal Carbonyls*; Wender, I., Pino, P., Eds.; Wiley: New York, 1977; Vol. II, pp 43–135.
(3) Heck, R. F.; Breslow, D. S. *J. Am. Chem. Soc.* **1961**, *83*, 4023.
(4) (a) Noack, K.; Calderazzo, F. J. *J. Organomet. Chem.* **1967**, *10*, 101. (b) Wojcicki, A. *Adv. Organomet. Chem.* **1973**, *11*, 87. (c) McHugh, T. M.; Rest, A. J. *J. Chem. Soc., Dalton Trans.* **1980**, 2323. (d) Berke, H.; Hoffmann, R. *J. Am. Chem. Soc.* **1978**, *100*, 7224. (e) Ziegler, T.; Versluis, L.; Tschinke, V. *J. Am. Chem. Soc.* **1986**, *108*, 612.
(5) (a) Lewis, K. E.; Golden, D. M.; Smith, G. P. *J. Am. Chem. Soc.* **1984**, *106*, 3906. (b) Connor, J. A. *Curr. Top. Chem.* **1977**, *71*, 71. (c) Ziegler, T.; Tschinke, V.; Ursenbach, C. *J. Am. Chem. Soc.* **1987**, *109*, 4825.
(6) McNeill, E. A.; Scholer, F. R. *J. Am. Chem. Soc.* **1977**, *99*, 6243.
(7) (a) Bellagamba, V.; Ercoli, R.; Gamba, A.; Suffritti, G. B. *J. Organomet. Chem.* **1980**, *190*, 381. (b) Grima, J. Ph.; Choplin, F.; Kaufmann, G. J. *J. Organomet. Chem.* **1977**, *129*, 221. (c) Fonnesbech, N.; Hjortkjaer, J.; Johansen, H. *Int. J. Quantum Chem.* **1977**, *12*, 95. (d) Fonnesbech, N. Ph.D. Thesis, Denmark Technical University, Copenhagen, 1979. (e) Pensak, D. A.; McKinney, R. J. *Inorg. Chem.* **1979**, *18*, 3407. (f) Eyermann, C. J.; Chung-Phillips, A. *J. Am. Chem. Soc.* **1984**, *106*, 7437.
(8) (a) Sweany, R. L.; Russell, F. N. *Organometallics* **1988**, *7*, 719. (b) Antolovic, D.; Davidson, E. R. *J. Am. Chem. Soc.* **1987**, *109*, 5828. Antolovic, D.; Davidson, E. R. *J. Am. Chem. Soc.* **1987**, *109*, 977. (c) Antolovic, D.; Davidson, E. R. *J. Chem. Phys.* **1988**, *88*, 4967. (d) Veillard, A.; Strich, A. *J. Am. Chem. Soc.* **1988**, *110*, 3793. (e) Daniel, C.; Hyla-Kryspin, I.; Demuynck, J.; Veillard, A. *Nouv. J. Chim.* **1985**, *9*, 581.

0002-7863/89/1511-2018$01.50/0 © 1989 American Chemical Society

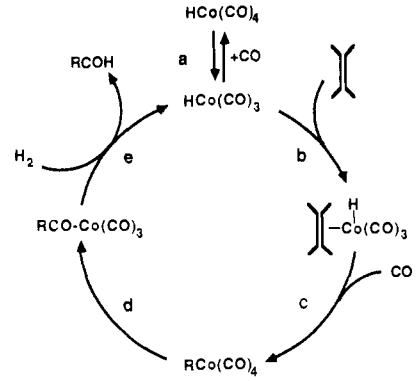

Figure 1. Schematic representation of the cobalt-based catalytic cycle for the hydroformylation reaction.

We shall here present a study on the steps a and d based on the Hartree–Fock–Slater (HFS) method[10] in the implementation due to Baerends et al.[11] There are two main points that we would like to address. The first is concerned with the geometries and relative stabilities of the possible conformers for the precatalyst $HCo(CO)_4$ and the catalytic active hydrido complex $HCo(CO)_3$ as well as the reaction enthalpy of step a. The second point is concerned with the reaction enthhalpy of step d with R = CH_3 as well as the possible structures of $CH_3Co(CO)_4$ and $CH_3C(O)Co(CO)_3$. Attention will in addition be given to the migratory insertion process d in which R = CH_3 has been replaced with R = H. We shall finally attempt to trace by an approximate linear transit procedure[12] the energy profile of d for the case where CH_3 migrates to a *cis*-carbonyl ligand as well as the case where CO inserts into the Co–CH_3 bond.

Several studies have shown that the HFS method provides M–L[13] (and M–M)[14] bond distances in close agreement with experiment, and all structure optimizations in the present investigation were carried out by a newly developed algorithm[15] based on energy gradients. This algorithm has been tested on several systems, including $HCo(CO)_4$. The HFS method has further been applied successfully in conjunction with Becke's nonlocal exchange correction,[16] to calculations on M–L (M–M)[17] bond energies with L = CO,[5c] H,[17b] and CH_3 as well as other ligands.[17a]

II. Computational Details

All calculations were based on the LCAO–HFS method as implemented by Baerends et al.[11] and extended with nonlocal exchange corrections[16] as well as corrections to allow for correlation of electrons between different spins.[18] The bonding energies were calculated by the generalized transition-state method.[19] Use was made of the fully vectorized version of the LCAO–HFS program of Ravenek.[11b]

An uncontracted triple-ζ STO basis set[20] was used for cobalt. The ligand atoms were represented by a double-ζ STO basis set[20] extended with one polarization function (2p on H and 3d on C and O). The 1s electrons on C and O as well as the 1s, 2s, and 2p electrons on Co were considered as core electrons and treated by the frozen-core approximation according to Baerends et al.[11] The total molecular electron density was fitted in each SCF iteration by atom-centered s, p, d, f, and g STO functions in order to represent the Coulomb and exchange potentials accurately.[21]

All molecular structures were optimized fully within the C_s symmetry group at the HFS level of approximation. The geometry optimization procedure was based on a standard quasi-Newton minimization technique utilizing analytical energy gradients.[15] Becke's nonlocal exchange correction was employed in connection with M–CO bond energy calculations.

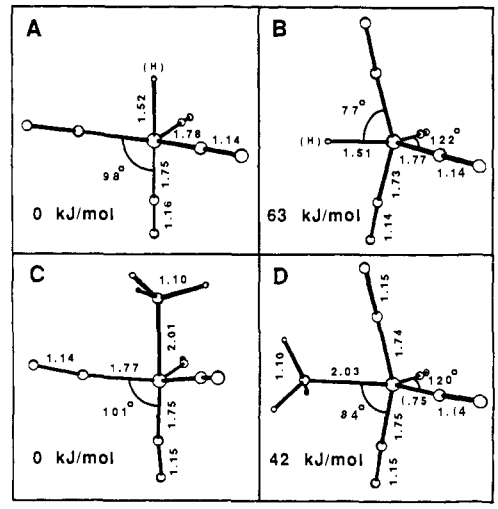

Figure 2. Optimized structures and relative energies of $RCo(CO)_4$ for R = H and R = CH_3. The energies of A and C are arbitrarily set to zero. The energies of B and D are relative to A and C, respectively. Bond distances are in angstroms. (A) C_{3v}-$HCo(CO)_4$; (B) C_{2v}-$HCo(CO)_4$; (C) C_{3v}-$CH_3Co(CO)_4$; (D) C_{2v}-$CH_3Co(CO)_4$.

Table I. Structural Data on $HCo(CO)_4$ from Experiment, HF Calculations, and HFS Calculations

	expt[a]	HF[b]	HFS[c]
$R(Co-CO_{ax})$[d]	1.764 (10)	2.02	1.753
$R(Co-CO_{eq})$	1.818 (8)	1.96	1.779
$R(C-O)_{av}$	1.141 (3)	1.12	1.141
R(Co–H)	1.556 (18)	1.71	1.516
$\theta(CO_{ax}-Co-CO_{eq})$[e]	99.7 (6)		97.6

[a] Reference 6. [b] Reference 8. [c] Reference 15. [d] All bond distances are in angstroms. [e] In degrees.

III. Molecular and Electronic Structure of $RCo(CO)_4$ (R = H, CH_3)

We find, in agreement with experiment,[6] that $HCo(CO)_4$ has a trigonal-bipyramidal (TBP) structure of C_{3v} symmetry (**1a**) with

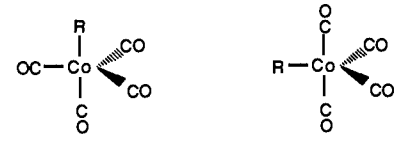

1a **1b**

the hydride in the axial position. The fully optimized C_{3v} structure of $HCo(CO)_4$ is given in Figure 2A. The alternative TBP conformation (**1b**) with the hydride in the equatorial position (Figure

(9) (a) Lüthi, H. P.; Siegbahn, P. E. M.; Almlof, J. *J. Phys. Chem.* **1985**, *89*, 2156. (b) Lüthi, H. P.; Ammeter, J. A.; Almlof, J.; Faegri, K. *J. Chem. Phys.* **1982**, *77*, 2002. (c) Faegri, K.; Almlof, J. *Chem. Phys. Lett.* **1984**, *107*, 121. (d) Almlof, J.; Faegri, K.; Schilling, B. E. R.; Lüthi, H. P. *Chem. Phys. Lett.* **1984**, *106*, 266.

(10) Slater, J. C. *Adv. Quantum Chem.* **1972**, *6*, 1.

(11) (a) Baerends, E. J.; Ellis, D. E.; Ros, P. *Chem. Phys.* **1973**, *2*, 71. (b) Ravenek, W. In *Algorithms and Applications on Vector and Parallel Computers*; Riele, H. J. J., Dekker, Th. J., van de Vorst, H. A., Eds.; Elsevier: Amsterdam, 1987.

(12) Salem, L. In *Electrons in Chemical Reactions*; Wiley: New York, 1982. (b) Komornicki, A.; McIver, J. W. *J. Am. Chem. Soc.* **1974**, *96*, 5798.

(13) (a) Becke, A. C. *J. Chem. Phys.* **1982**, *76*, 6037. (b) Dunlap, B. I. *J. Phys. Chem.* **1986**, *90*, 5524. (c) Baerends, E. J.; Rozendaal, A. In *Quantum Chemistry: The Challenge of Transition Metals and Coordination Chemistry*; NATO ASI Series, Series C; Veillard, A., Ed.; Reidel: Dordrecht, 1985; Vol. 176, p 159. (d) Rösch, N.; Jörg, H.; Dunlap, B. I. In *Quantum Chemistry: The Challenge of Transition Metals and Coordination Chemistry*; NATO ASI Series, Series C; Veillard, A., Ed.; Reidel: Dordrecht, 1985; Vol. 176, p 179.

(14) (a) Ziegler, T. *J. Am. Chem. Soc.* **1984**, *106*, 5901. (b) Ziegler, T. *J. Am. Chem. Soc.* **1983**, *105*, 7543. (c) Ziegler, T. *J. Am. Chem. Soc.* **1985**, *107*, 4453.

(15) Versluis, L.; Ziegler, T. *J. Chem. Phys.* **1988**, *88*, 322.

(16) Becke, A. *J. Chem. Phys.* **1986**, *84*, 4524.

(17) (a) Ziegler, T.; Tschinke, V.; Versluis, L.; Baerends, E. J. *Polyhedron*, in press. (b) Ziegler, T.; Tschinke, V.; Becke, A. *J. Am. Chem. Soc.* **1987**, *109*, 1351.

(18) Stoll, H.; Golka, E.; Preuss, H. *Theor. Chim. Acta* **1980**, *55*, 29.

(19) Ziegler, T.; Rauk, A. *Theor. Chim. Acta* **1977**, *46*, 1.

(20) (a) Snijders, G. J.; Baerends, E. J.; Vernooijs, P. *At. Nucl. Data Tables* **1982**, *26*, 483. (b) Vernoois, P.; Snijders, G. J.; Baerends, E. J. "Slater Type Basis Functions for the Whole Periodic System", Internal Report, Free University of Amsterdam, The Netherlands, 1981.

(21) Krijn, J.; Baerends, E. J. "Fit Functions in the HFS Method, Internal Report (in Dutch), Free University of Amsterdam, The Netherlands, 1984.

2B) was calculated to be 63 kJ mol^{-1} higher in energy. The structure of $CH_3Co(CO)_4$ is not known in detail. We find that $CH_3Co(CO)_4$ of conformation **1a** is 42 kJ mol^{-1} lower in energy than $CH_3Co(CO)_4$ of conformation **1b**; see Figure 2C,D.

The electronic structure of $HCo(CO)_4$ as well as that of other d^8 TBP complexes has been studied[7] extensively, and we[17b] have recently analyzed the relative strengths of the Co–H and Co–CH_3 bonds in $RCo(CO)_4$ (R = H, CH_3). The only other theoretical structure investigation involving a full geometry optimization is the ab initio HF study[8] by Antolovic and Davidson. We compare in Table I structural parameters from HF and HFS calculations with experiment. It follows from Table I that the Co–CO and Co–H bond distances calculated by the HF method are too large by 0.2 and 0.1 Å, respectively. The HFS method provides, on the other hand, distances that are too short by 0.03 Å. The results in Table I are quite typical in that M–L bond distances calculated by the HF method generally[9] are much too large, in particular when L is a π-acceptor, whereas M–L bond distances calculated[13,15] by the HFS method are somewhat too short. The HF study finds in addition $HCo(CO)_4$ in the two conformations **1a** and **1b** to be similar in energy, in contrast to experiment and the present HFS investigation. The optimized structures in Figure 2 have very few striking features. The axial and equatorial Co–CO bond distances are quite similar (±0.03 Å), and the equatorial CO_{eq}–Co–CO_{eq} bond angles are in all cases close to 120°. We find further the Co–R distances to be quite similar (±0.03 Å) in the two conformations **1a** and **1b**, in contrast to the HF study,[8] in which R(Co–H_{ax}) = 1.71 Å and R(Co–H_{eq}) = 1.59 Å for R = H. The only distinct feature in Figure 2 is the bending of the axial CO ligands toward R. We refer to the work by Elian and Hoffmann[22] for an elegant analysis of the bending motion of the axial ligands as well as the factors favoring **1a** over **1b** in the case of $HCo(CO)_4$. An analysis of our calculations on $HCo(CO)_4$ in conformation **2b** shows that the stabilization, which results from

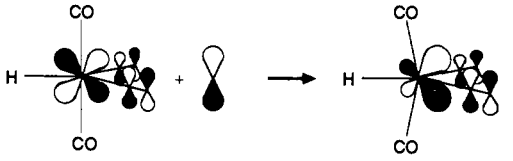

2a 2b

bending the axial carbonyls toward the equatorial position (CO_{ax}–Co–CO_{ax} = 180° → 150°), primarily (80%) can be attributed to a relief in steric interactions between the CO ligands. Electronically, the bending motion allows the $4p_z$ and $3d_{xz}$ metal orbitals to mix (**2a**), and the resulting pd hybrid is seen (**2b**) to be polarized toward the two equatorial π^*_{CO} orbitals away from the hydride, which lacks π-acceptor orbitals. The bending will as a result enhance the π-back-donation in the equatorial plane. A similar bending has recently been observed and rationalized in $M(CO)_4(C_2H_2)$ (M = Fe, Ru, Os).[23]

IV. Molecular and Electronic Structure of $HCo(CO)_3$

The initial key step in the hydroformylation process is according to Figure 1 represented by the dissociation of a CO ligand from $HCo(CO)_4$. The dissociation process results in the formation of the catalytically active species $HCo(CO)_3$ (eq 1). The dissociation

$$HCo(CO)_4 \rightarrow HCo(CO)_3 + CO \qquad (1)$$

is assumed to take place prior to, or in concert with, the complexation of an olefin leading to the olefinic π-complex $HCo(CO)_3(\eta^2$-olefin) (Figure 1b). The coordinatively unsaturated 16-electron species $HCo(CO)_3$ has been identified by matrix isolation techniques,[24] but its structure is unknown.

We shall here discuss the possible conformations of the $HCo(CO)_3$ species produced from the dissociation in eq 1. Our investigation will be confined to singlet states of $HCo(CO)_3$ since

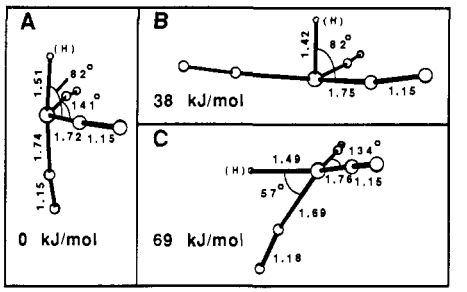

Figure 3. Optimized structures and relative energies of $HCo(CO)_3$. The energies of B and C are relative to A, which was set arbitrarily to zero. Bond distances are in angstroms.

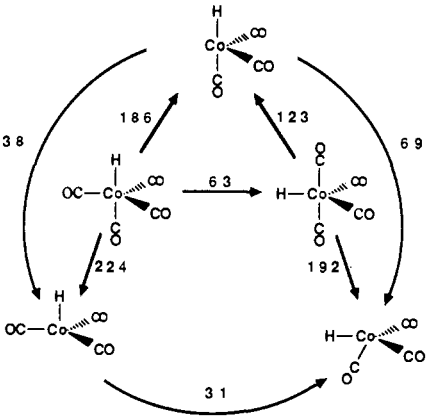

Figure 4. Energy requirements for the interconversions of the isomers of $HCo(CO)_4$ and $HCo(CO)_3$ as well as the CO dissociation of $HCo(CO)_4$. All energies are in kJ mol^{-1}.

the carbonyl-exchange process most likely takes place on the singlet surface.[8c-e] Dissociation of either an equatorial or an axial CO ligand from $HCo(CO)_4$ in its ground-state conformation (**1a**) gives rise to **3a** and **3b**, respectively. Both **3a** and **3b** constitute in our

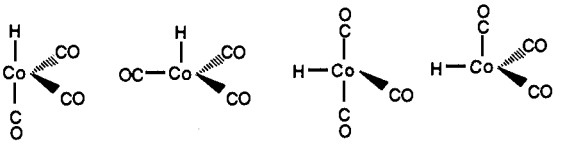

3a 3b 3c 3d

calculations local minima on the singlet surface of $HCo(CO)_3$, and the optimized structures are shown in Figure 3. We calculate $HCo(CO)_3$ with the butterfly shape (**3a**) to be 38 kJ mol^{-1} lower in energy than the trigonal-shaped $HCo(CO)_3$ species **3b**. The equatorial (**1a** → **3a**) and axial (**1a** → **3b**) CO dissociation energies were found to be 186 and 224 kJ mol^{-1}, respectively. The CO dissociation energies for the d^8 complex $HCo(CO)_4$ are not known experimentally. Our calculated values compare, however, well with an experimental[25] (singlet) dissociation energy in the d^8 complex $Fe(CO)_5$ of 183 kJ mol^{-1}. The energetics for the process in eq 1 has been summarized in Figure 4.

The C_{2v} structure (**1b**) of $HCo(CO)_4$ is according to our calculations 63 kJ mol^{-1} higher in energy than the C_{3v} structure (**1a**) of $HCo(CO)_4$. A CO dissociation from **1b** should as a consequence not be of importance for the carbonyl–olefin exchange reaction (b of Figure 1). We have, however, for the sake of completeness considered the two products **3c** and **3d**, generated from the cleavage of respectively an equatorial and axial CO ligand in **1b**. The structure **3c** does not constitute a local minimum on the potential (singlet) surface of $HCo(CO)_3$ according to our calculations but converges on optimization to **3a** (Figure 3A) by a pseudorotation. Conformation **3d** (Figure 3C) represents a local minimum with an energy of 69 kJ mol^{-1} above **3a**. The axial (**1a**

(22) Elian, M.; Hoffmann, R. *Inorg. Chem.* **1975**, *14*, 1058.
(23) Ball, R. G.; Burke, M. R.; Takats, J. *Organometallics* **1987**, *6*, 1918.
(24) Wermer, P.; Ault, B. S.; Orchin, M. *J. Organomet. Chem.* **1978**, *162*, 189.
(25) Lewis, K. E.; Golden, D. M.; Smith, G. P. *J. Am. Chem. Soc.* **1984**, *106*, 3906.

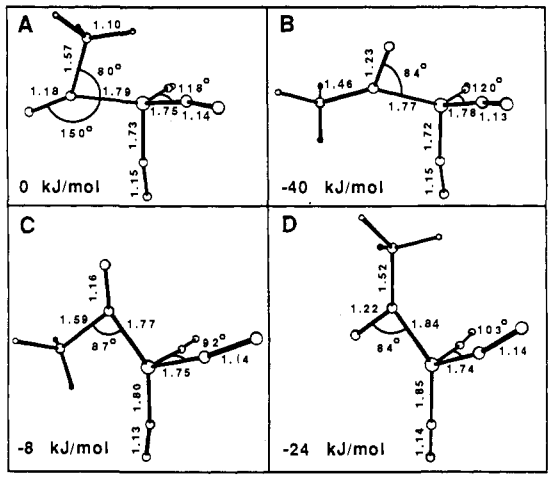

Figure 5. Optimized structures and relative energies of $CH_3C(O)Co(CO)_3$. The energies are relative to structure A, which was set arbitrarily to zero. All bond distances are in amgstroms. (A) η^1-$CH_3C(O)Co(CO)_3$ with $CH_3C(O)$ in equatorial position; (B) η^2-$CH_3C(O)Co(CO)_3$ with $CH_3C(O)$ in equatorial position; (C) η^1-$CH_3C(O)Co(CO)_3$ with $CH_3C(O)$ in axial position; (D) η^2-$CH_3C(O)Co(CO)_3$ with $CH_3C(O)$ in axial position.

→ **3d**) and equatorial (**1b** → **3c**) dissociation energies were calculated as 192 and 123 kJ mol^{-1}, respectively (Figure 4). $HCo(CO)_3$ of conformation **3d** (Figure 3C) has as the parent C_{2v}-shaped hydride $HCo(CO)_4$ (Figure 2B) with the axial CO ligand bent toward the hydride. This bending can, as in the case of Figure 2B, be attributed to steric interactions (see section III).

Both **3b** and **3c** are accessible from the optimal butterfly structure **3a** of $HCo(CO)_3$ by rotation of respectively the axial CO or H ligand. We have not determined the energy barrier of interconversion. It is, however, clear that a major part of the barrier will stem from the repulsive four-electron interaction between the occupied d_{xz} metal orbital and the occupied σ_{1s} or σ_{CO} orbitals on the axial H and CO ligands, respectively (**4**). It should be noted that the optimal structure of $HCo(CO)_3$ is ideally suited for π-interaction with an olefin.

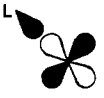

4

Some experimental evidence for the existence of $HCo(CO)_3$ in different configurations was given in a recent publication by Sweany and Russell,[8a] who infer, based on results of the photolysis of $HCo(CO)_4$ in an argon matrix, that $HCo(CO)_3$ forms two isomers consistent with structures **3a** and **3b**. Antolovic and Davidson[8b] have also examined the singlet structure of $HCo(CO)_3$. They find that **3a**, **3b**, and **3d** as well as **3c** represent local minima. The spread in energy between the four conformations in the HF study was only 18 kJ mol^{-1}, with **3d** as the more stable structure. The close proximity of the energies for the four conformations **3a–d** in the HF study is most likely a consequence of the fact that the HF method in contrast to experiment finds the two structures of $HCo(CO)_4$ (**1a** and **1b**) to be of almost equal stability, with structure **1b** lower in energy than **1a**. The HF study finds the Co–CO bond distance in $HCo(CO)_3$ to be even longer (1.97–2.12 Å) than in the parent $HCo(CO)_4$ molecules. In a recent follow-up study by the same authors,[8c] $HCo(CO)_4$ was investigated at the SDCI level of theory. Although no new geometry optimization was performed, the authors find, in agreement with our results, the order of stability of **1a** and **1b** for $HCo(CO)_4$ to be inverted. Antolovic and Davidson have also discussed the structure of $HCo(CO)_3$ in the triplet state.

V. Electronic and Molecular Structure of $CH_3(O)CCo(CO)_3$

The formation of $HCo(CO)_3$ is in Figure 1 followed by π-complexation of an olefin to $HCo(CO)_3$ (b of Figure 1) and the subsequent insertion of the olefin into the Co–H bond (c of Figure 1) by which the alkyl complex $RCo(CO)_4$ is formed. The two steps b and c will be studied in a later investigation on the homologation of alcohols, and we shall here proceed to an analysis of step d in which the acyl complex $RC(O)Co(CO)_3$ is formed from $RCo(CO)_4$ by a migratory insertion of the alkyl group R into the Co–CO bond. The migratory insertion of R into the M–CO bond has been inferred as a key step in several processes. There are, however, only limited experimental data available on the migration process. It has in particular not been possible experimentally to study the energetics for the migration process d of Figure 1. Furthermore, the structures of the intermediates involved in step d are not known in any detail.

We have studied the structures of the acyl intermediates that arise from a migratory insertion reaction of the methyl group in $CH_3Co(CO)_4$ under the constraint of C_s symmetry. Reaction d of Figure 1 can, as we will see in more detail in section VI, proceed along two conceivable pathways. The first process involves the migration of the alkyl group from its equilibrium position to a *cis*-carbonyl ligand as displayed in eq 2. Alternatively, the alkyl

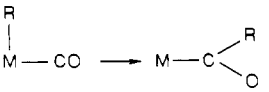

(2)

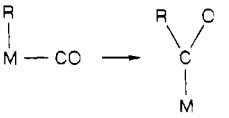

(3)

to acyl conversion can also occur by an insertion of a carbon monoxide ligand into the metal–alkyl bond according to eq 3. Both of these reaction modes are potentially accessible to $CH_3Co(CO)_4$ with configurations **5a** and **6a**. The resulting acyl intermediates are represented by structures **5b**, **5c**, **6b**, and **6c**, respectively.

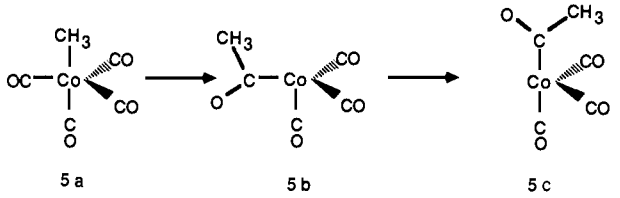

5a **5b** **5c**

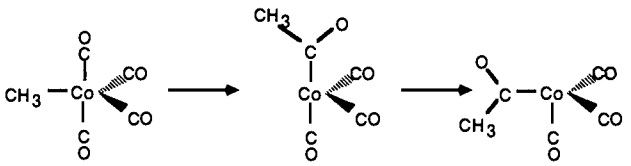

6a **6b** **6c**

We have optimized the four acyl species fully and find all of them to represent true minima on the HFS energy surface (Figure 5). We find complex **6c**, with the acyl group in the equatorial position and the acyl oxygen atom facing the vacant site, to be lowest in energy. Structures **5c**, **6b**, and **5b** are higher in energy by 16, 32, and 40 kJ mol^{-1}, respectively. The higher stability of complex **6c** and **5c** compared to **6b** and **5b** can be ascribed to the formation of a stable η^2 interaction (see Figure 5B,D). The lone-pair electrons of the acyl oxygens of structures **6c** and **5c** can in both cases interact with low-lying unoccupied orbitals polarized along the axis of the empty site (**7a** and **7b**). Orbital **7a** arises

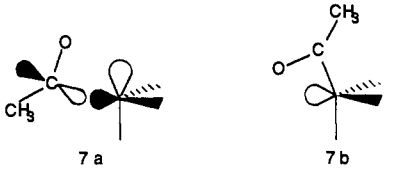

7a **7b**

mainly from the antibonding interaction between $2a'_{OCCH_3}$ and

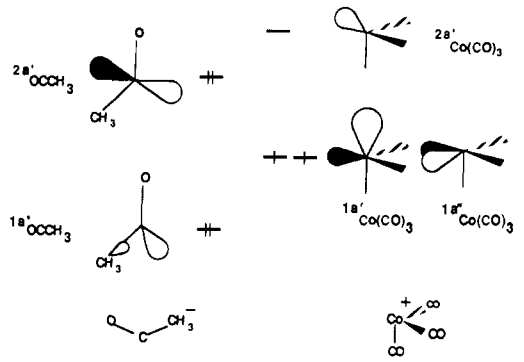

Figure 6. Frontier orbitals of the fragments $CH_3C(O)^-$ and $Co(CO)_3^+$.[4d]

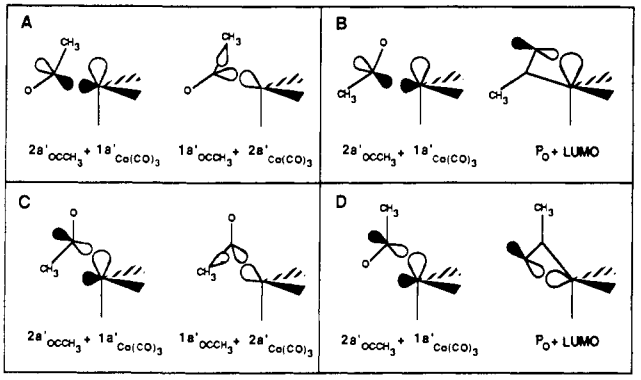

Figure 7. Schematic representation of the bonding interactions between the $CH_3C(O)^-$ and $Co(CO)_3^+$ fragments for structures **5b**, **5c**, **6b**, and **6c**.

$1a'_{Co(CO)_3}$ of Figure 6, while **7b** is formed from orbital $2a'_{Co(CO)_3}$, which is primarily 4p in character,[22] by mixing in a second p function (**8**).

8

The lower stability of complex **5c** with respect to **6c** is somewhat surprising since **5c** derives its main stabilization from the interaction of $2a'_{OCCH_3}$ of Figure 6 with the larger lobe of $1a'_{Co(CO)_3}$ (Figure 7B), while the corresponding orbital of structure **6c** overlaps with the smaller lobe of $1a'_{Co(CO)_3}$ (Figure 7D). However, in order for **5c** to form a stabilizing η^2 interaction, the axial acyl ligand must bend toward the empty orbital polarized along the equatorial position. This motion causes an unfavorable four-electron destabilization between the acyl σ-orbital ($2a'_{OCCH_3}$ of Figure 6) and a nonbonding occupied d-type orbital (**9**).

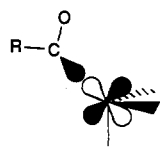

9

The stabilization of complex **5c** compared to **6c** is further reduced by a weaker η^2 interaction between the lone-pair electrons of the acyl oxygen of **5c** and orbital **7b**. An analysis of our data reveals that the interaction between the p-orbital of the acyl oxygen and orbital **7a** of **6c** is about 20 kJ mol^{-1} stronger than for the corresponding interaction of **5c**.

It should be noted here that the η^2 structure is unlikely to form under catalytic reaction conditions, since the coordinatively unsaturated acyl intermediate readily can bind a CO or H_2 molecule. However, in support of our results Sweany[26] reports the apparent formation of an η^2-acyl complex in a low-temperature matrix study of the photolysis of $CH_3C(O)Co(CO)_4$.

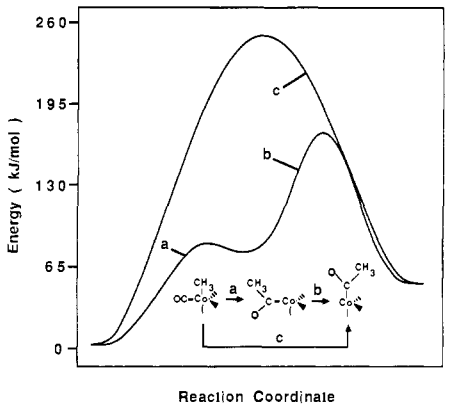

Figure 8. Energy profiles of the alkyl to acyl conversions of C_{3v}-$CH_3Co(CO)_4$ under C_s symmetry constraints. The energy zero point refers to C_{3v}-$CH_3Co(CO)_4$ (**5a**). (a) Methyl migration **5a** → **5b**; (b) Acyl conversion to the η^2 structure, **5b** → **5c**; (c) direct insertion of CO into the Co-CH_3 bond of C_{3v}-$CH_3Co(CO)_4$, **5a** → **6c**.

Complexes **5b** and **6b** are structurally very similar to **6c** and **5c**, respectively. The bond angle between the methyl carbon, the acyl carbon, and the metal center, $\theta(C_{CH_3}-C_{acyl}-Co)$, of **5b** and **6c** is, however, with 80° unexpectedly small. This angle results from the interaction of orbital $1a'_{OCCH_3}$ of Figure 6 with $2a'_{Co(CO)_3}$, since tilting the acyl group toward the vacant site maximizes the overlap between $1a'_{OCCH_3}$ and $2a'_{Co(CO)_3}$ as illustrated in Figure 7A,C. The stability and the closeness of relative energies of the acyl complexes **5b**, **5c**, **6b**, and **6c** suggest that all four of them are likely candidates for intermediates of the migratory insertion step d of Figure 1. In the next section we shall investigate the actual migration process.

VI. Migratory Insertion Step

We shall here study the energy profile for the migratory insertion process d with $CH_3Co(CO)_4$ as a model compound. The energy profiles will be constructed in an approximate fashion by a linear variation of all internal coordinates from reactant to product. This linear transit procedure[12] affords an upper bound to the actual activation energy for the process. The migratory insertion step d can be envisioned to take place either as a migration of the methyl group to a *cis*-CO ligand (e.g., **5a** → **5b**) or as an insertion of a CO ligand into the Co-CH_3 bond (e.g., **5a** → **5c**). Both reaction modes will be considered here. Attention will be given to processes involving $CH_3Co(CO)_4$ in conformation **5a** as well as **6a** although the discussion in section III would indicate that **5a** is the more stable structure for $RCo(CO)_4$.

The reaction profile for the methyl migration (**5a** → **5b**) with the more stable C_{3v} complex **5a** as the initial structure is given in Figure 8a. The profile in Figure 8a corresponds to a migration of the CH_3 group under the constraint of C_s symmetry. We find for **5a** → **5b** an endothermicity ΔH of 71 kJ mol^{-1} and a very modest activation barrier $\Delta E^{\ddagger}$ of only 9 kJ mol^{-1}. These results compare well with an earlier study[4e] on the CH_3 to CO migration in $CH_3Mn(CO)_5$ where we found ΔH to be 75 kJ mol^{-1} and $\Delta E^{\ddagger}$ to be 11 kJ mol^{-1}. Our findings are also in agreement with a recent kinetic study by Roe,[32] who found the rate constant of the methyl back-migration of $CH_3C(O)Co(CO)_3$ to be considerably larger than the rate constant for the corresponding forward reaction. The 9 kJ mol^{-1} calculated for $\Delta E^{\ddagger}$ by the linear transit is an upper bound to the actual value, and we can thus conclude that the methyl migration (**5a** → **5b**) should proceed with a rather modest activation barrier.

Another plausible mechanism for step d, in which methyl migration is involved, would be the conversion of $CH_3Co(CO)_4$ from its equilibrium structure **5a** to the less stable conformation **6a**, followed by a migration of the equatorial CH_3 group to an

(26) Sweany, R. L. *Organometallics*, submitted for publication.

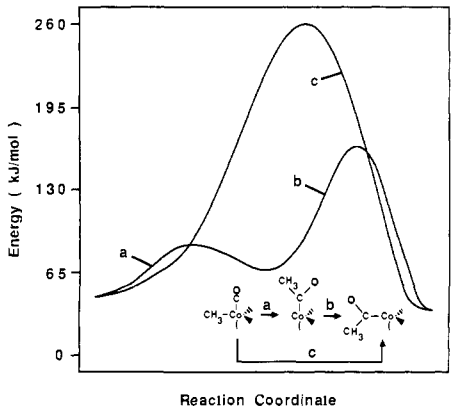

Figure 9. Energy profiles of the alkyl to acyl conversions of C_{2v}-$CH_3Co(CO)_4$ under C_s symmetry constraints. The energy zero point refers to C_{3v}-$CH_3Co(CO)_4$ (**5a**). (a) Methyl migration **6a** → **6b**; (b) acyl conversion to the η^2 structure, **6b** → **6c**; (c) direct insertion of CO into the Co–CH_3 bond of C_{3v}-$CH_3Co(CO)_4$, **6a** → **6c**.

axial CO ligand (**6a** → **6b**) under C_s constraint. An energy profile for the methyl migration (**6a** → **6b**) is given in Figure 9a. The process **6a** → **6b** is less endothermic than **5a** → **5b**, with a ΔH of 21 kJ mol^{-1}. The activation barrier is, on the other hand, somewhat larger, with a $\Delta E^{\ddagger}$ of 19 kJ mol^{-1}. The combined sequence **5a** → **6a** → **6b** has a reaction enthalpy of 63 kJ mol^{-1}.

Relaxation of the C_s constraint gives rise to a number of additional processes involving methyl migration. They will not be considered here. We shall instead conclude that the two processes **5a** → **5b** and **5a** → **6a** → **6b** have sufficiently modest enthalpies and barriers to be likely candidates as reaction modes for step d of Figure 1. In fact, d will not be the rate-limiting step in the hydroformylation process if the migratory insertion d proceeds along **5a** → **5b** or **5a** → **6a** → **6b**, since the CO dissociation in step a of Figure 1 (section IV) has a reaction enthalpy of ~200 kJ mol^{-1}.

We consider next the alternative mechanism for d in which $CH_3Co(CO)_4$ is converted into an acyl complex by the insertion of a CO ligand into the Co–CH_3 bond. The calculated energy profiles for the carbonyl insertion into the axial (**5a** → **5c**) and equatorial (**6a** → **6c**) methyl–cobalt bonds are given in Figures 8c and 9c, respectively. The axial insertion process (**5a** → **5c**) has an enthalpy of 47 kJ mol^{-1} and a barrier of 195 kJ mol^{-1}. The corresponding values for the equatorial insertion (**6a** → **6c**) are −11 and 245 kJ mol^{-1}, respectively. The reaction barriers for the two CO insertion processes are thus seen to be much higher than the barriers for the methyl migrations.

The high energy barriers arise mainly from the departure of the carbonyl ligand from its stable equilibrium position. Thus, the CO insertion process rotates the carbonyl molecule toward the methyl group, thereby inflicting a four-electron destabilization between the occupied σ_{CO} orbital and a nonbonding d-orbital. The energy barriers in Figures 8c and 9c are enhanced further by the fission of the methyl–cobalt bond and the cleavage of the π^*_{CO} back-bonding interaction. The destabilizing factors mentioned here should also be present in a more synchhronous transit, and we would thus expect the actual barriers for the CO insertion processes **5a** → **5c** and **6a** → **6c** to be substantial, although reduced somewhat from those based on the linear transits in Figures 8c and 9c.

The enthalpies for the insertion reactions are seen to be smaller than the corresponding values for the migration processes. This is understandable since the acyl complexes **5c** and **6c** are more stable than the acyl complexes **5b** and **6b** (see Figures 5 and 10). In fact, the CO migration process (**6a** → **6c**) in which the less stable conformation **6a** of $CH_3Co(CO)_4$ is converted into the most stable conformation **6c** of $CH_3C(O)Co(CO)_3$ has a negative reaction enthalpy of −11 kJ mol^{-1}. The results presented in Figures 8c and 9c would indicate that the CO insertion, although thermodynamically favorable, is an unlikely candidate as a mechanism for step d due to its high activation barrier.

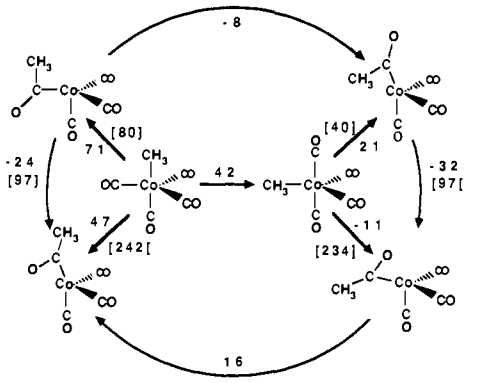

Figure 10. Energy requirements for the alkyl to acyl conversion of $CH_3Co(CO)_4$ as well as the interconversions of the isomers of $CH_3Co(CO)_4$ and $CH_3C(O)Co(CO)_3$. All energies are in kJ mol^{-1}. The numbers in brackets represent the activation energies for the reactions in the direction of the arrows. The numbers without brackets stand for the energy difference between two isomers, where a positive value indicates that the resulting complex is higher in energy.

The acyl products **5b** and **6b**, from the more favorable methyl migrations, are of higher energy than the two η^2 conformations **5c** and **6c** from the CO insertions, and we shall here, in order to round off the picture, consider possible routes for the rearrangements of **5b** and **6b** into **5c** and **6c**. It is, however, important to point out that such rearrangements are unlikely to occur under standard catalytic conditions[2] of 200–300 atm and 100–200 °C of CO + H_2 where the coordinatively unsaturated acyl complex $CH_3Co(CO)_3$ would be quenched in a reaction with either CO or H_2 (step e of Figure 1).

Energy profiles for the acyl conversions **5b** → **5c** and **6b** → **6c** are also given in Figures 8 and 9, where we can compare now the reaction sequences **5a** → **5b** → **5c** and **6a** → **6b** → **6c** with the direct CO insertion reactions **5a** → **5c** and **6a** → **6c**. The acyl conversion processes were modeled by moving the acyl group from the basal to the apical orientation (**5b** → **5c**) and vice versa (**6b** → **6c**) under C_s constraint. It follows from Figures 8 and 9 that the two acyl conversion processes have an activation barrier of 97 kJ mol^{-1}. Further, the two-step reactions **5,6a** → **5,6b** → **5,6c** are seen to be more favorable (lower barrier) than the CO insertion reactions **5,6a** → **5,6c**.

VII. Molecular and Electronic Structure of $(COH)Co(CO)_3$

We have in the previous section discussed the 1,2-shift reaction of an alkyl group in which a metal–alkyl system is converted into a metal–acyl complex (e.g., **5a** → **5b**). This type of reaction is well documented for a variety of alkyl complexes. The corresponding 1,2-shift reaction (e.g., **10a** → **10b**) involving H rather than alkyl has proven, on the other hand, to be rather elusive. The 1,2-hydride-shift reaction, which in earlier work was inferred[27,28] as an elementary reaction step, has in spite of considerable efforts only been detected with certainty in a few cases.[29] It is now widely accepted that the hydride migration, in contrast to the alkyl migration, is thermodynamically unfavorable at least for middle to late transition metals.

We have studied the two 1,2-shift reactions **10a** → **10b** and **11a** → **11b**. The first reaction (**10a** → **10b**) represents a 1,2-shift of a hydride in $HCo(CO)_4$ with C_{3v} symmetry and the second reaction (**11a** → **11b**) the corresponding shift of a hydride in $HCo(CO)_4$ with C_{2v} symmetry. We have found that neither of the formyl structures **10b** or **11b** represents local energy minima on the HFS energy surface. Thus any attempt to optimize the two structures **10b** and **11b** resulted in a back-migration of the

(27) (a) Dombek, B. D. *Ann. N.Y. Acad. Sci.* **1983**, *415*, 176. (b) Dombek, B. D. In *Adv. Catal.* **1983**, *32*, 325.
(28) Byers, B. H.; Brown, T. L. *J. Am. Chem. Soc.* **1977**, *99*, 2527.
(29) (a) Wayland, B. B.; Duttahmed, A.; Woods, B. A.; Pierce, R. *J. Chem. Soc., Chem. Commun.* **1983**, 143–144. (b) Fagan, P. J.; Manriquers, J. M.; Marks, T. J.; Vollmer, S. H.; Day, C. S.; Day, V. W. *J. Am. Chem. Soc.* **1981**, *103*, 2206. (c) Moloy, K. G.; Marks, T. J. *J. Am. Chem. Soc.* **1984**, *106*, 7051.

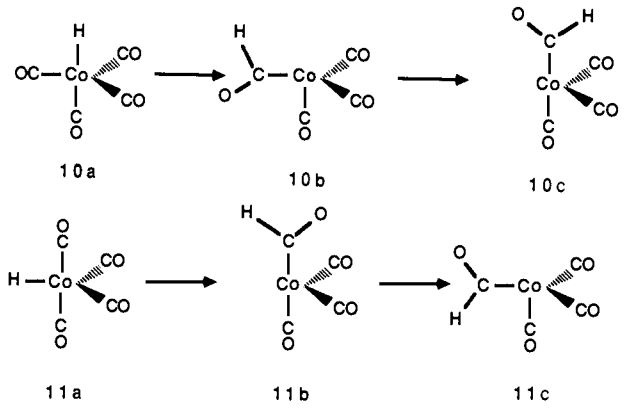

formyl hydrogen to the parent hydrido metal complexes **10a** and **11a**, respectively. Our findings would indicate that the two formyl complexes **10b** and **11b** are kinetically unstable with respect to the parent hydrido complexes. That is, the two decarbonylation reactions **10b** → **10a** and **11b** → **11a** should have at most a minimal activation barrier. Our findings can be reconciled with the experimental observation that most neutral metal formyl complexes decarbonylate readily to the corresponding hydrido complexes.[30] The decomposition is believed to occur by a back-migration of the formyl hydrogen to the metal center under loss of a ligand of the coordinatively saturated formyl complex. The stability of the formyl complex depends not only on the relative stability of the coordinatively unsaturated intermediate but also on the dissociation energy of the coligands. We have calculated the carbonyl–cobalt bond energy of $HC(O)Co(CO)_4$ (a of Figure 12) to be 133 kJ mol^{-1}. This value agrees well with what is typically found for the M–CO bond strength of middle to late d^8 first-row transition-metal complexes.[31] However, Roe[32] found in a recent study an activation energy of only ~80 kJ mol^{-1} for the CO dissociation of $CH_3C(O)Co(CO)_4$, which implies that the CO–Co bond strength is close to or lower than this value. The discrepancy between his estimate of the bond energy and our calculation arises from the fact that we have not allowed for relaxation effects of the fragments during the dissociation process. Inclusion of the latter reduces the calculated CO–Co dissociation energy of $HC(O)Co(CO)_4$ to 82 kJ mol^{-1}, as is depicted by reaction b of Figure 12. The coordinatively unsaturated intermediate that is formed from the CO dissociation (a of Figure 12) can, as described before, rearrange to the parent hydrido complex without a significant activation barrier. This rearrangement of the intermediate to $HCo(CO)_4$ of structure **11a** (e of Figure 12) was calculated to lower the energy by 139 kJ mol^{-1}. Since structure **11a** can readily interconvert (i of Figure 12) to the more stable form of $HCo(CO)_4$ with the hydrogen atom in the apical position (**10a**), the decarbonylation of $HC(O)Co(CO)_4$ (eq 4) becomes a facile process with an exothermicity of $\Delta H = -69$ kJ mol^{-1}.

$$HC(O)Co(CO)_4 \rightarrow HCo(CO)_4 + CO \qquad (4)$$

Acyl complexes are, in contrast to their formyl counterparts, well-known molecules. We have not calculated the CO–Co bond energy of $CH_3C(O)Co(CO)_4$, but it is reasonable to assume that the dissociation energy D(CO–Co) is similar for acyl and formyl compounds. The rearrangement energy for the methyl back-migration, on the other hand, was calculated to be substantially lower (~70 kJ mol^{-1}) than for the corresponding hydride migration (e of Figure 12). This difference can (see later) be correlated to the difference between the Co–H and Co–CH_3 bond

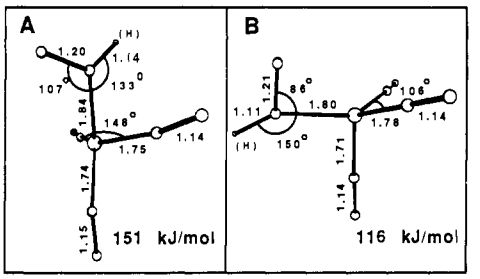

Figure 11. Optimized structures and relative energies of $HC(O)Co(C-O)_3$. The energies are relative to C_{3v}-$HCo(CO)_4$ (**1a** for R = H). All bond distances are in angstroms. (A) η^1-$HC(O)Co(CO)_3$ with HC(O) in axial position; (B) η^2-$HC(O)Co(CO)_3$ with HC(O) in equatorial position.

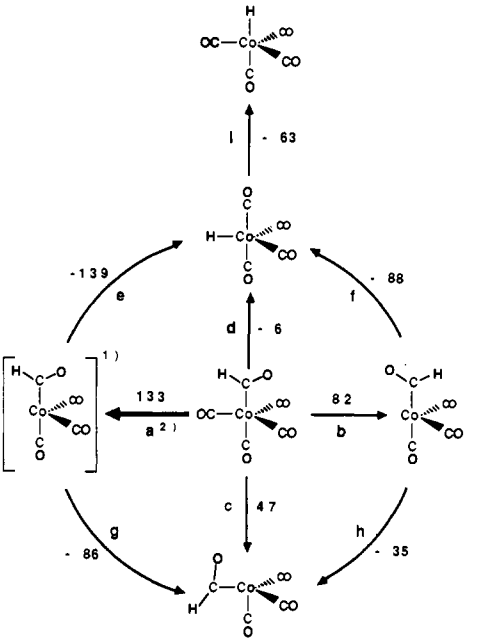

Figure 12. Energy requirements for the decarbonylation reaction of $HC(O)Co(CO)_4$ to $HCo(CO)_4$. All energies are in kJ mol^{-1}. (1) Intermediate not stable on the HFS energy surface; (2) Co–CO dissociation energy without allowing the fragments to relax.

strengths. $CH_3Co(CO)_4$ of structure **6a** can relax further to the more stable configuration **5a**; however, the decarbonylation process of $CH_3C(O)Co(CO)_4$ remains endothermic with $\Delta H \approx 20$ kJ mol^{-1}. Thus the acyl complex is thermodynamically stable, while the formyl analogue is unstable and decomposes to $HCo(CO)_4$ according to eq 4. The isoelectronic d^8 formyl complex $HC(O)Fe(CO)_4^-$ has been found to decompose slowly to $HFe(CO)_4^-$.[33a] The kinetic stability can probably be ascribed to the stabilization of the M–CO bond due to increased back-bonding interactions of the carbonyl ligands in the charged species. However, the overall reaction is thermodynamically favorable, with a reported exothermicity of $\Delta H = -43 \pm 30$ kJ mol^{-1}.[33b]

Our results are in disagreement with the recent HF study where Antolovic and Davidson find the two structures **10b** and **11b** to represent local minima with activation energies for the decarbonylation processes **10b** → **10a** and **11b** → **11a** of 120 and 158 kJ mol^{-1}, respectively.

We have also investigated the structures of the two formyl complexes **10c** and **11c**. The two structures **10c** and **11c** are in principle accessible from **10a** and **11a**, respectively, either by a two-step reaction (**10,11a** → **10,11b** → **10,11c**) or by a direct insertion of a CO ligand into the Co–H bond (**10,11a** → **10,11c**).

The optimized structures for the two formyls **10c** and **11c** are given in Figure 11, parts A and B, respectively. We find that **10c**

(30) (a) Tam, W.; Wong, W. K.; Gladysz, J. A. *J. Am. Chem. Soc.* **1979**, *101*, 1589. (b) Collins, T. J.; Roper, W. R. *J. Chem. Soc., Chem. Comm.* **1976**, 1044. (c) Brown, K. L.; Clark, G. R.; Headford, C. E. L.; Marsden, K.; Roper, W. R. *J. Am. Chem. Soc.* **1979**, *101*, 503. (d) Chaudret, B. N.; Cole-Hamilton, D. J.; Nohr, R. S.; Wilkinson, G. *J. Chem. Soc., Dalton Trans.* **1977**, 1546.

(31) (a) Skinner, H. A.; Connor, J. A. *Pure Appl. Chem.* **1985**, *57*, 79. (b) Tschinke, V.; Ziegler, T. In *Density Matrices and Density Functionals*; Erdahl, R. M., Smith, V. H., Jr. Eds.; Reidel: Dordrecht, 1987.

(32) Roe, D. C. *Organometallics* **1987**, *6*, 942.

(33) (a) Collman, J. P.; Winter, S. R. *J. Am. Chem. Soc.* **1973**, *95*, 4089. (b) Lane, K. R.; Sallans, L.; Squires, R. R. *Organometallics* **1985**, *4*, 408.

with the formyl group along the apical axis is 35 kJ mol^{-1} higher in energy than **11c** with the formyl group along the equatorial axis. The higher stability of **11c** compared to **10c** can be attributed to the lack of η^2 interaction in **10c** (see later). The two formyl complexes **10c** and **11c** are respectively 151 and 53 kJ mol^{-1} higher in energy than the parent hydrido complexes **10a** and **11a**. Thus the formyl intermediates are by 104 and 64 kJ mol^{-1} more endothermic than the corresponding acyl compounds **5c** and **6c** with respect to the migration reaction. The higher endothermicity of the hydride migration can largely be ascribed to the higher bond strength of Co–H compared to Co–CH_3. For middle to late transition metals D(M–H) is ~240 kJ mol^{-1} whereas the corresponding D(M–CH_3) bond strength only is ~160 kJ mol^{-1}. The stability of **10c** is in comparison to **5c** further reduced by the failure of complex **10c** to form a stabilizing η^2 structure. **10c** (Figure 11A) is also structurally quite different from its acyl analogue **5c** (Figure 5D). Most notably, as mentioned above, is the absence of an η^2 interaction. In order to form an η^2 interaction, the formyl group of complex **10c** has to bend toward the basal position (see section V). This motion causes a four-electron destabilization between the σ_{HCO} orbital of thhe formyl group and a nonbonding d-type orbital of the central metal (**9**). Our results seem to indicate that, for the formyl complex **10c**, the destabilizing effect overpowers the energy stabilization that would result from an η^2 formation. Thus complex **10c** does not adopt an η^2-formyl structure but keps the bond angle between the axial carbon atoms and the metal center (θ(C_{ax}–Co–C_{ax})) at 180°. We find in addition that the bond angle between the equatorial carbons and the cobalt nucleus θ(C_{eq}–Co–C_{eq}) of **10c** is substantially larger than for the corresponding acyl compound **5c**. The opening of the C_{eq}–Co–C_{eq} bond angle was predicted by Berke and Hoffmann,[4d] who explain this effect by the reduction of the antibonding interaction between a d-type orbital of the metal center and the σ-orbitals of the carbonyl ligands (**12**).

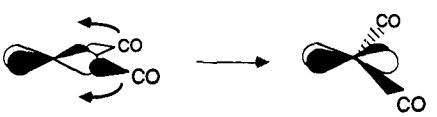

12

The acyl analogue of **10c**, complex **5c**, on the other hand, keeps the bond angle θ(C_{eq}–Co–C_{eq}) small (103°). Reducing θ(C_{eq}–Co–C_{eq}), **13a** → **13b**, from 180° to a smaller angle allows the $3d_{z^2}$

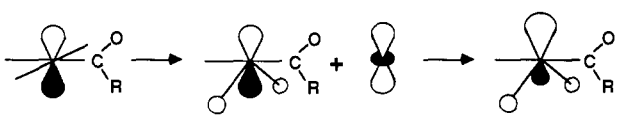

13a 13b 13c

metal orbital to mix (**13b**) with the $4p_z$ orbital, which largely constitutes the LUMO for a d^8 square-planar system.[22] The resulting hybrid **13c** reduces the antibonding interaction between $4p_z$ and the ligand σ-orbitals, and more importantly, the pd hybrid is now polarized away from the equatorial carbonyls, which results in an increased overlap with the lone-pair electrons of the acyl oxygen atom. Thus a small bond angle between the equatorial carbons and the metal center enhances the η^2 stabilization of the acyl intermediate **5c**.

Our results suggest that kinetically stable coordinatively unsaturated formyl complexes with geometry **10c** or **11c** could exist. The experimental observations that most of these compounds undergo decarbonylation to the corresponding hydrido complexes can probably be ascribed to a facile interconversion of **10c** and **11c** to the unstable structures **10b** and **11b** by a pseudorotation. However, complexes of geometry **10c** and **11c** might, as in the acyl case, be observed in low-temperature matrix experiments.

VIII. Summary and Conclusions

We have studied here two of the reaction steps of the cobalt-based catalytic cycle of the hydroformylation process, namely, reaction a of Figure 1, where the precatalyst $HCo(CO)_4$ is converted to the catalytic active species $HCo(CO)_3$ by a CO dissociation, and reaction d of Figure 1, where an acyl intermediate is formed from $RCo(CO)_4$ by a migratory insertion of CO into the R–Co bond.

The structural parameters of $RCo(CO)_4$ were determined for R = H and R = CH_3, respectively. Both complexes were found to form two stable isomers of trigonal-bipyramidal geometry. The C_{3v} structures of $RCo(CO)_4$ with R along the apical axis were found to be 63 and 42 kJ mol^{-1} lower in energy than the C_{2v} isomers with R in the basal position for R = H and R = CH_3, respectively. The coordinatively unsaturated catalyst $HCo(CO)_3$ was shown to have three stable isomers. Thhe one lowest in energy has a butterfly-shaped geometry (**3a**) with hydrogen in the trans position. This configuration is ideally suited for π-interactions with incoming olefins, and it can be reached directly by a dissociation of an equatorial CO ligand of $HCo(CO)_4$ in either configuration (**1a** or **1b**). The CO dissociation energy was found to be 186 kJ mol^{-1} for **1a** → **3a** and 123 kJ mol^{-1} for **1b** → **3a**.

The migratory insertion step d of Figure 1 was investigated by a linear transit procedure using $CH_3Co(CO)_4$ as a model compound. There are four acyl intermediates that can result from a migratory conversion of $CH_3Co(CO)_4$ with configuration **1a** or **1b** under C_s symmetry constraints. All four of them were found to be stable on the HFS surface, with the ones that have the acyl oxygen facing the vacant site lowest in energy due to the formation of stable η^2 interactions. We have modeled the reaction paths of the alkyl to acyl conversion and found the migration of the methyl group to a *cis*-carbonyl ligand of $CH_3Co(CO)_4$ in either configuration to have a low activation barrier and a reaction enthalpy of not more than 70 kJ mol^{-1}. The direct insertion of a CO ligand into the CH_3–Co bond was, in contrast, disfavored by a high activation barrier of ~200 kJ mol^{-1}. We conclude that the migratory insertion reaction (d of Figure 1) is a likely key step of the catalytic cycle, since the acyl intermediates are stable species and can be reached by reaction paths that have modest activation barriers and reaction enthalpies. In fact, the migratory insertion reaction will not be the rate-determining step, since the CO dissociation (a of Figure 1) has a far higher reaction enthalpy.

We have further investigated the products of the migratory insertion reaction, d of Figure 1, for R = H. We found that neither of the formyl intermediates that resulted from a direct migration of the hydride to a carbonyl group were stable on the HFS energy surface. The configurations with the formyl oxygen facing the vacant site were found to be stable but considerably higher in energy than their acyl analogues with respect to the parent $RCo(CO)_4$ system. Thus, the 1,2-shift reaction of $HCo(CO)_4$ was found to be a thermodynamically as well as kinetically unfavorable process.

Finally, we also have discussed briefly the stability of the coordinatively saturated complex $RC(O)Co(CO)_4$ for R = H and R = CH_3, respectively. The formyl complex was, in contrast to its acyl counterpart, found to be thermodynamically unstable with respect to decarbonylation to the parent hydrido complex.

Acknowledgment. This investigation was supported by the National Science and Engineering Research Council of Canada (NSERC) through a grant to T.Z. We thank the Killam Foundation for a scholarship to L.V. All calculations were carried out at the Cyber-205 installation of the University of Calgary.

Registry No. 1a (R = H), 64519-62-6; $CH_3Co(CO)_4$, 14709-64-9; $HCo(CO)_3$, 60105-25-1; $CH_3(O)CCo(CO)_3$, 118920-03-9; $(HCO)Co(CO)_3$, 118920-04-0; $HC(O)Co(CO)_4$, 118920-05-1; $MeC(O)Co(CO)_4$, 13964-92-6.